

Direct Grid Connection of a Slip-Permanent Magnet Wind Turbine Generator

U. Hoffmann, P. Bouwer and M.J. Kamper
Department of Electrical and Electronic Engineering
University of Stellenbosch
Stellenbosch, South Africa
Email: kamper@sun.ac.za

Abstract—The slip-permanent magnet generator offers potential for direct-driven, direct-to-grid sub-100 kW wind turbine generators. This reduces complexity and cost, as well as maintenance requirements. A major challenge, however, is to synchronise the generator to the grid without the benefit of turbine torque control. This paper presents the simulation and testing of a synchronisation controller designed to achieve this goal. Simulations are used to determine acceptable conditions for synchronisation and to evaluate two speed control approaches, based on loading the generator with a resistor bank. A thyristor-based control strategy is shown to operate effectively, even under turbulent wind conditions. Experimental tests of the system show that the synchronisation mechanism works correctly – good agreement with simulation results is achieved.

I. INTRODUCTION

This investigation focuses on small-scale (sub-100 kW) grid-connected wind turbine generators (WTGs). Such systems can find application in developing nations where infrastructure, investment and available support services are limited. Affordability is an especially high priority because cost has been identified as one of the most significant barriers to the uptake of renewable energy technology in the developing world [1]. Reliability, efficiency and grid support capabilities are also important parameters when selecting an appropriate WTG topology for this application.

The slip-permanent magnet generator (S-PMG) described in [2] can be connected directly to both the wind turbine and the electrical grid. This sets it apart from other grid-connected topologies, such those making use of doubly-fed induction generators (DFIGs) and converter-fed synchronous generators (SGs), shown in Fig. 1.

Through the use of a two-stage design, the S-PMG avoids the need for costly secondary components such as a gearbox and a frequency converter – items which also affect reliability and maintenance [3]. In addition, the S-PMG has better on-grid characteristics than an IG because it can assist in maintaining voltage stability by providing grid fault response similar to conventional SGs [4].

Direct grid connection is generally problematic for synchronous WTGs because the torque angle of an SG directly affects its power output – this results in a propensity for low-frequency oscillations and instability [5]. In contrast, the S-PMG is stable during wind fluctuations [4]. This is due to the inclusion of a slip-rotor, illustrated in Fig. 2, which allows for

slip between the turbine and the synchronous PM-rotor. As a result, the S-PMG acts as a low-pass filter against torque disturbances introduced by wind turbulence.

A challenge with the S-PMG concept is synchronising the generator under dynamically variable conditions without relying upon blade pitch control to regulate turbine torque output. Literature provides limited insight into the problem since previous investigations into the direct grid connection of SG-based WTGs have centred around medium to large generators [6]–[9] where some means of torque control has typically been available.

This paper proposes a design for the synchronisation controller (SC) that performs the monitoring, speed control and synchronisation of the S-PMG under variable wind conditions. The synchronisation tolerance window is determined and a speed control system is developed with the aid of numerical simulations. The SC design is then verified through laboratory experiments.

A. Comparison of the S-PMG with a Converter-fed PMSG

The converter-fed PMSG, shown in Fig. 1(b), is an appealing option in terms of efficiency and controllability. External field excitation is not required so the PMSG offers higher efficiency at low wind speeds. Maximum power-point tracking (MPPT) is also possible due to variable speed operation of the generator.

The primary disadvantage of the PMSG is its reliance on a full-scale frequency converter, which has serious cost and reliability implications and seldom operates at rated capacity. The S-PMG does away with the need for a converter and only requires a mechanism to synchronise it with the grid. In both systems, capital cost and mechanical wear can be reduced by avoiding the use of a gearbox, as well as pitch and yaw control.

In comparison, the PMSG requires a higher initial investment but can be expected to capture more energy per annum due to MPPT, whereas the S-PMG operates at virtually fixed speed when connected to the grid. The difference in energy capture between fixed and variable speed WTGs has been shown in [10] to depend strongly on the nature of the wind site and can be expected to range from 8 to 15% [11]. The S-PMG will perform comparatively well at sites with relatively high, steady wind speeds.

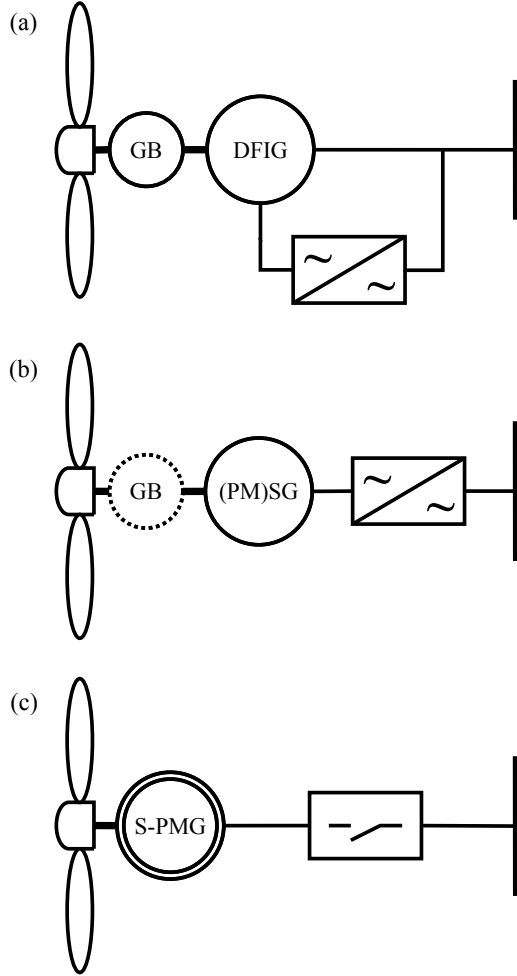


Fig. 1. A selection of grid-connected WTG Topologies: (a) DFIG with gearbox and partial-scale frequency converter, (b) SG or PMSG with full-scale frequency converter and optional gearbox, and (c) S-PMG with synchronisation controller

Overall, the S-PMG offers the potential for a more robust and affordable WTG implementation. With fewer vulnerable components, the risk of down-time and expensive repairs is reduced. Through optimisation of design and material usage, the total S-PMG system cost can also be lower than that of an equivalent converter-fed system. Finally, the S-PMG naturally exhibits grid fault response similar to conventional SGs and does not pose the risk of introducing switching harmonics on to weak grids.

B. S-PMG Operating Principle

As Fig. 2 shows, the S-PMG is a radial-flux machine that consists of a slip-rotor connected to the turbine, a freely rotating permanent-magnet rotor, and a grid-connected stator. These parts form two fully distinct stages.

The slip-rotor and the associated side of the PM-rotor constitute the first stage: a short-circuited synchronous machine that develops substantial torque as soon as the slip speed ω_{sle}

is non-zero (ω_{sle} is defined as the difference between the electrical velocities of the PM-rotor ω_{me} and slip-rotor ω_{re}).

The second stage, a conventional multi-pole PMSG, is formed by the stator and its associated side of the PM-rotor. This stage is driven by the torque produced by the slip-rotor when $\omega_{sle} > 0$. When the machine is connected directly to the grid, the PM-rotor operates at synchronous speed ω_b , whereas the slip-rotor remains capable of speed excursions, dependent on loading conditions.

The value of this two-stage design becomes apparent when examining a spring-mass-damper analogy of the electro-mechanical system [7]. Fig. 3(a) shows that a grid-connected PMSG is virtually undamped and thus prone to long-term oscillations. In contrast, the S-PMG in Fig. 3(b) will exhibit damped behaviour as long as the PM-rotor to stator connection is stiffer than the slip-rotor to PM-rotor connection. The turbine to slip-rotor connection is very stiff due to the absence of a gearbox or even a connecting shaft.

Under the stated conditions, the turbine-slip-rotor subsystem oscillates against the PM-rotor-stator subsystem whenever a disturbance is experienced. Such oscillations are, however, rapidly attenuated because the connection between the two subsystems is sufficiently damped. In this way the S-PMG achieves damping similar to that offered by damper windings, which are considered to be difficult to implement in high pole-number PMSGs [7].

The operational procedure of the proposed S-PMG system, starting from rest, is as follows:

- 1) The wind is relied upon to produce enough torque in the turbine to accelerate the system from rest.
- 2) The speed and/or rate of acceleration of the S-PMG is regulated by an electrical braking system (shown schematically in Fig. 2 and described in Section IV). This system consists of the resistive load R_d and the switch S1, which is controlled by the MCU.
- 3) Once the synchronisation conditions are satisfied, as explained in Section III, the S-PMG is connected directly to the grid by closing switch S2.

II. MODELLING

A. Turbine and Turbulent Wind

The turbine under consideration is a horizontal axis type with a diameter of 7.2 m – its power curves are summarised in Fig. 4. Yaw error is considered negligible for the purposes of simulation.

Both steady and turbulent wind inputs are considered, with turbulent wind signals synthesized according to [12]. The time-dependent turbulent wind input and the turbine response (as a function of wind and turbine speed) are implemented in simulation using look-up tables.

B. S-PMG

The S-PMG is described using *VHDL-AMS* with its electrical system modelled in the PM-rotor synchronous dq reference

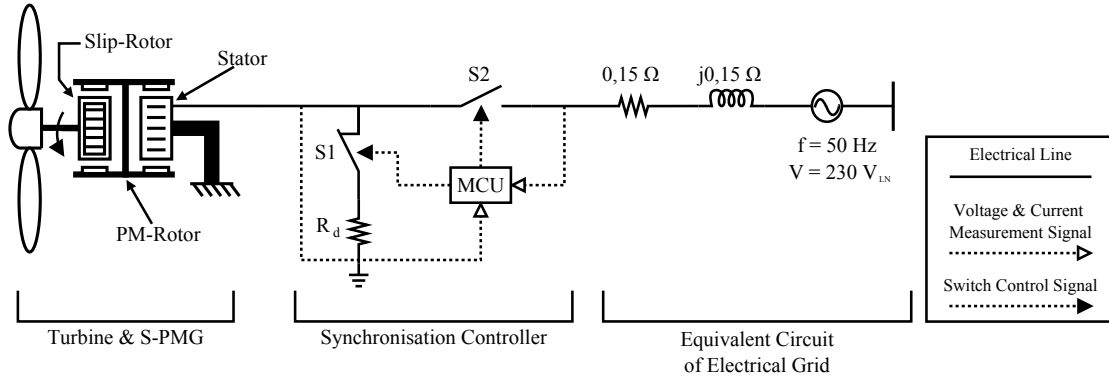


Fig. 2. Schematic of the S-PMG, synchronisation controller, and per-phase equivalent circuit model of the grid

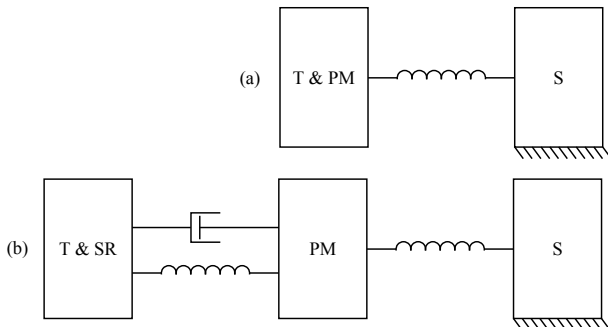


Fig. 3. Spring-Mass-Damper analogy for (a) PMSG and (b) S-PMG. Rotational masses: 'T' = Turbine, 'PM' = PM-Rotor, 'S' = Stator, and 'SR' = Slip-Rotor. Original concept from [7]

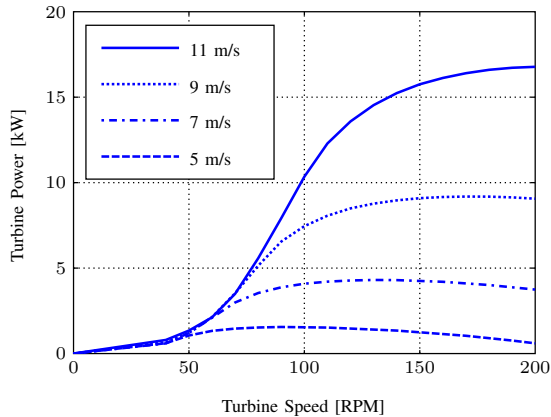


Fig. 4. Turbine power curves as a function of turbine speed for different wind speeds. Rated power is obtained at 150 rpm with a wind speed of 11m/s

frame [4]. Equations (1) and (2) govern the electrical dynamics of the slip-rotor, while (3) and (4) do so for the stator.

$$0 = -i_{qr}R_r - L_{qr} \frac{di_{qr}}{dt} - \omega_{sle}L_{dr}i_{dr} + \omega_{sle}\lambda_{mr} \quad (1)$$

$$0 = -i_{dr}R_r - L_{dr} \frac{di_{dr}}{dt} + \omega_{sle}L_{qr}i_{qr} \quad (2)$$

$$v_{qs} = -i_{qs}R_s - L_{qs} \frac{di_{qs}}{dt} - \omega_{me}L_{ds}i_{ds} + \omega_{me}\lambda_{ms} \quad (3)$$

$$v_{ds} = -i_{ds}R_s - L_{ds} \frac{di_{ds}}{dt} + \omega_{me}L_{qs}i_{qs} \quad (4)$$

Equations (5) and (6) describe the electromagnetic torque generated by the slip-rotor and the stator respectively. The mechanical dynamics of the two independently rotating sections are governed by (7) and (8). In all cases, subscript t refers to the turbine, r the slip-rotor, m the PM-rotor, and s the stator. The additional subscript e explicitly indicates an electrical quantity. All simulations are conducted in Ansoft *Simplorer*.

$$T_r = \frac{3}{4}p[(L_{qr} - L_{dr})i_{dr}i_{qr} + \lambda_{mr}i_{qr}] \quad (5)$$

$$T_s = \frac{3}{4}p[(L_{qs} - L_{ds})i_{ds}i_{qs} + \lambda_{ms}i_{qs}] \quad (6)$$

$$T_t = J_t \frac{d\omega_t}{dt} + B_t\omega_t + T_r \quad (7)$$

$$T_m = T_r - T_s = J_m \frac{d\omega_m}{dt} + B_m\omega_m \quad (8)$$

C. Control Elements and Electrical Grid

The MCU-based SC has access to 3-phase voltage and current measurements on both grid and generator side. The MCU has a sampling rate of 1 kHz and is able to actuate thyristors through a delay angle generator, as well as contactors. The v - i characteristic of the thyristors is described by an equivalent line model. The contactors are modelled as perfect switches with a 14 ms actuation delay. The dumping load R_d is treated as a purely resistive, wye-connected load.

The grid is modelled by an equivalent circuit, shown in Fig. 2, with impedance according to [13]. Grid voltage and frequency disturbances originating outside the S-PMG system are not considered in this study.

III. SYNCHRONISATION

The synchronisation of the S-PMG to the grid entails a procedure similar to that employed for conventional SGs driven by steam or gas turbines. (In this case, however, control of excitation and maximum available torque is not possible.) To determine the appropriate instant to synchronise, the SC must compare aspects of the S-PMG and grid voltage waveforms.

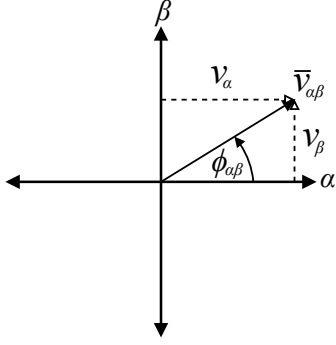


Fig. 5. Decomposition of $\bar{v}_{\alpha\beta}$ into v_α and v_β

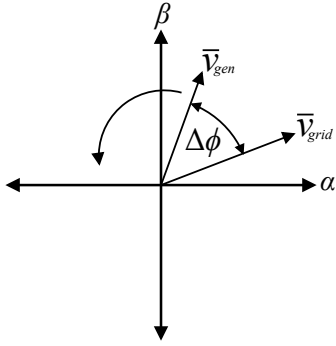


Fig. 6. Rotating $\alpha\beta$ voltage vectors

If a balanced three-phase system is assumed, comparison may be facilitated by transformation of the natural waveforms into the stationary $\alpha\beta$ reference frame:

$$\begin{bmatrix} v_\alpha \\ v_\beta \end{bmatrix} = \frac{2}{3} \begin{bmatrix} 1 & -0.5 & -0.5 \\ 0 & \frac{\sqrt{3}}{2} & -\frac{\sqrt{3}}{2} \end{bmatrix} \begin{bmatrix} v_a \\ v_b \\ v_c \end{bmatrix} \quad (9)$$

Fig. 5 shows that the transformed quantities v_α and v_β constitute orthogonal components of a rotating vector $\bar{v}_{\alpha\beta}$. The rotating vectors \bar{v}_{grid} and \bar{v}_{gen} , illustrated in Fig. 6, can be compared in real-time to evaluate the following conditions, which need to be met before synchronisation can occur:

- 1) Frequency difference: $\Delta f = |f_{grid} - f_{gen}| < f_t$
- 2) Magnitude difference: $\Delta v = ||\bar{v}_{grid}| - |\bar{v}_{gen}|| < v_t$
- 3) Angle difference: $\Delta\phi = |\phi_{grid} - \phi_{gen}| < \phi_t$

The synchronisation algorithm, based on the above three conditions, is depicted by the flow chart in Fig. 7. This algorithm is active throughout the operational wind speed range of 4 – 12 m/s. At mean wind speeds higher than this the turbine will overload the S-PMG so the system is set to engage standby mode until $V_{wind} \leq 12$ m/s.

Simulation studies were conducted to determine acceptable values for the tolerance band parameters f_t , v_t , and ϕ_t . Fig. 8a shows the effect of varying Δf on the maximum i_{rms} recorded during synchronisation and Fig. 8b does the same for $\Delta\phi$. The initial conditions for the simulations are: PM-rotor acceleration

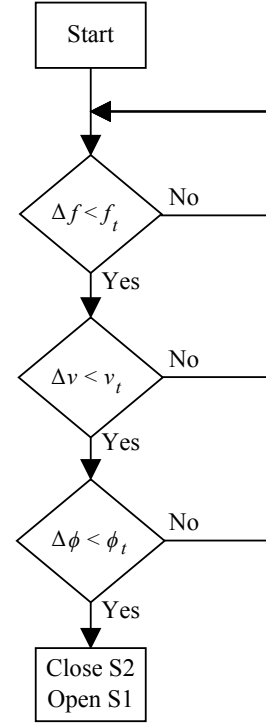


Fig. 7. Synchronisation logic

$\dot{\omega}_m = 0$ rad/s² and steady wind speed $V_{wind} = 4$ m/s. Because $\Delta v = f(\Delta f)$ for PMSGs, Δv was not investigated independently.

It is apparent from the simulation results that the transient current is a strong function of Δf , indicating that effective speed control is important to achieve successful synchronisation. In particular, tracking should be good under even turbulent conditions.

To ensure successful synchronisation, the following tolerance values have thus been selected: $f_t = 0.02$ p.u. and $\phi_t = 8^\circ$. These values are in fair agreement with the results of [7], [14], [15]. Fig. 8c shows that applying these limits will ensure that $i_{rms} < 2$ p.u. for synchronisation throughout the operational wind speed range.

IV. SPEED CONTROL

To ensure consistent synchronisation performance the required values of Δf and $\Delta\phi$ must be achieved reliably and quickly, irrespective of wind conditions. It is also desirable to minimise $\dot{\omega}_m$ at the moment of synchronisation. Ideally, $\dot{\omega}_m \approx 0$ rad/s² during synchronisation, but investigations have shown that $|\dot{\omega}_m| \leq 1$ rad/s² is acceptable.

The chosen method of speed control must be able to satisfy the requirements stated above, however, the cost and complexity of the system as a whole should not be unduly increased. Blade pitch control as a means of speed control is thus not suitable for small-scale systems. It has been decided instead to make use of a simple, robust electrical braking mechanism.

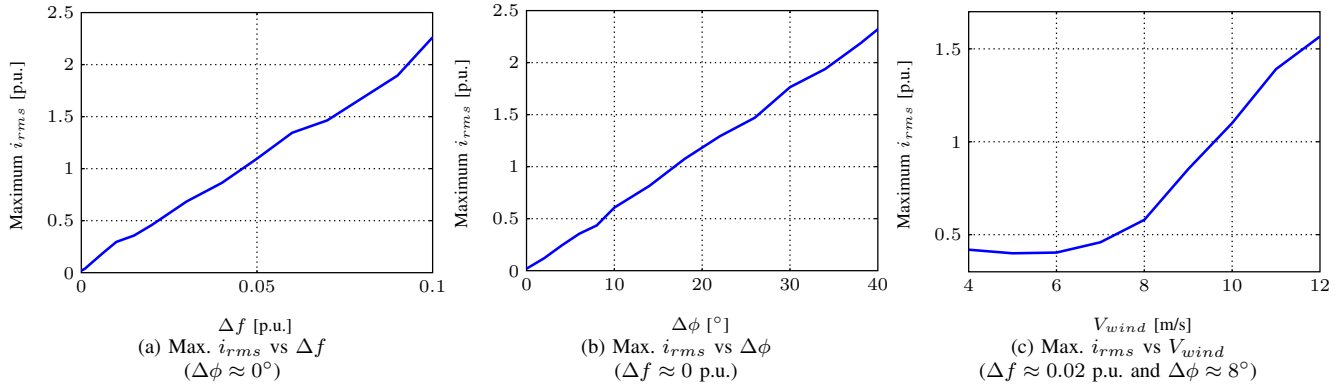


Fig. 8. Simulated effect of varying tolerance limits and wind speed at synchronisation

Equation (8) shows that the electromagnetic counter-torque T_s developed in the stator of the S-PMG can be used to control $\dot{\omega}_m$. By setting the electrical load imposed on the S-PMG, the stator currents and thus the torque T_s can be regulated, allowing fast speed control to be achieved.

A. Contactor-Based Speed Control

Different approaches can be used to switch in the resistive load R_d . The first option is to make use of a contactor to realise switch S1. This does not allow for dynamic speed control since only one resistance value can be switched in. Rather, the aim is to limit $\dot{\omega}_m$ when the S-PMG is in the correct frequency window ($\Delta f < f_t$) to synchronise by keeping S1 closed throughout the process.

Fig. 9 shows how the value of $\dot{\omega}_m$ (at $\Delta f = 0$ p.u.) changes as a function of wind speed with different values of R_d . It is clear that no single value of R_d will ensure that $|\dot{\omega}_m| \leq 1$ rad/s² across $4 \leq V_{wind} \leq 12$ m/s, however, applying no-load for $4 \leq V_{wind} \leq 7$ m/s and 40Ω for $7 < V_{wind} \leq 9$ m/s could achieve $|\dot{\omega}_m| \leq 1$ rad/s² for winds of 4 – 9 m/s. Additional contactors and load combinations would be necessary for a complete solution.

B. Thyristor-Based Speed Control

Replacing the contactor with thyristors allows for faster, repetitive switching without mechanical wear. The effective voltage imposed on R_d can be controlled by varying the firing delay angle in the range $0 \leq \alpha \leq 180^\circ$ in a continuous manner. This allows the counter-torque of the S-PMG to be changed incrementally, enabling the implementation of closed-loop speed control. The proposed control loop, employing a PI compensator, is shown in Fig. 10.

To avoid the use of additional sensors f_{gen} is to be measured by analysing the 3-phase S-PMG voltages, however, thyristor switching at intermediate α values leads to significant harmonic content in the voltage waveforms. This can result in a THD of more than 18%. The frequency measurement algorithm must thus be robust against harmonic interference.

Potential frequency determination techniques include: zero-crossing detection, filtered $\alpha\beta$ vector gradient, phase-locked

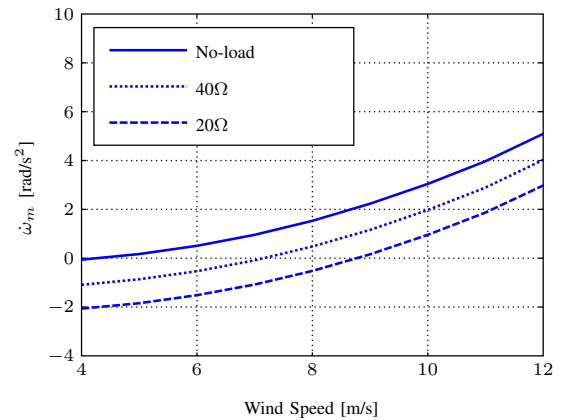


Fig. 9. Simulated PM-rotor acceleration through synchronous speed as a function of wind speed for different values of R_d

loop (PLL), and simplified Kalman observer (SKO) [16]. Determining $d\phi_{gen}/dt$ was found to be a convenient option since ϕ_{gen} is already calculated for synchronisation purposes. Low-pass filtering is required with this method but the computational burden is still relatively low.

After tuning, the following values were determined for the proportional and integral controller gains, respectively: $K_p = 15$ and $K_i = 20$. This configuration is designed to allow no more than 10% overshoot at winds up to 12 m/s. Fig. 11 shows that maximum predicted overshoot for steady wind at rated turbine torque is less than 5%. This is important for both controllability and over-voltage protection. Rise time and settling time, on the other hand, are strong functions of wind speed, which determines the maximum value of T_s available.

It was noted in Section III that accurate tracking is important to allow successful synchronisation. The turbulent wind sequence in Fig. 12 was used to test the tracking ability of the PI controller. The resulting PM-rotor speed as a function of time is shown in Fig. 13, which indicates that the controller is generally able to maintain $\Delta f < f_t$.

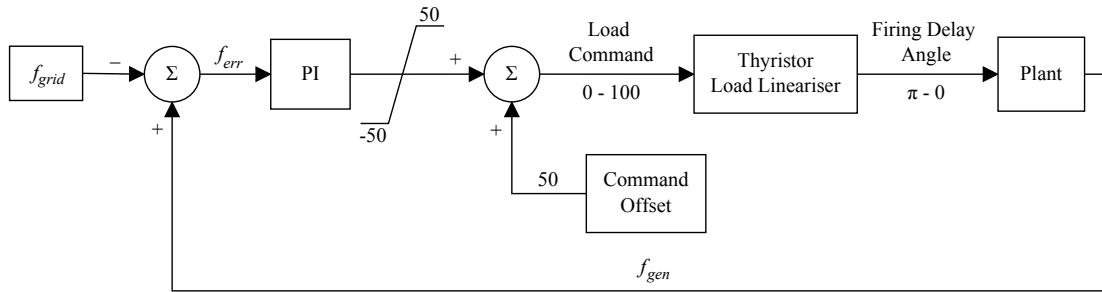


Fig. 10. PI Speed Control Loop

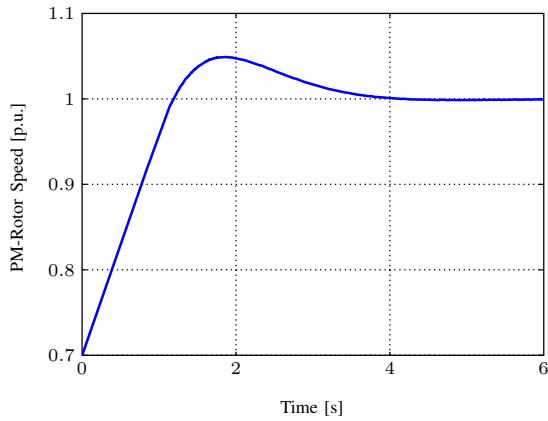


Fig. 11. Simulated PI speed control performance with $V_{wind} = 11$ m/s. Maximum overshoot is 4.9%

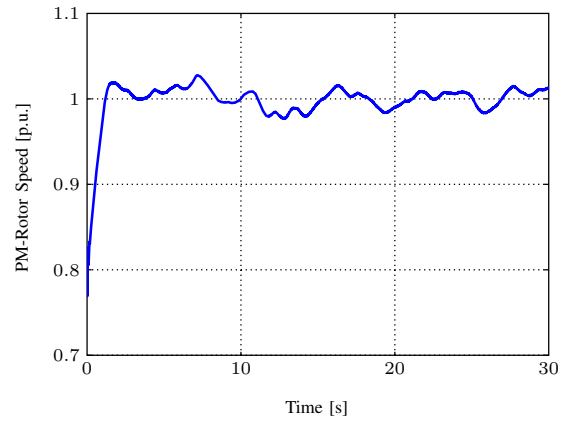


Fig. 13. Simulated PI speed control performance during turbulent wind

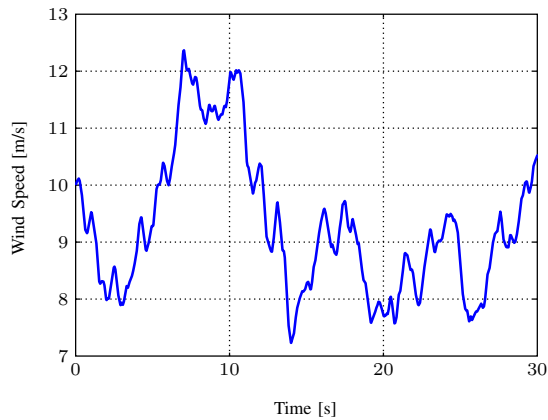


Fig. 12. Simulated turbulent wind sequence

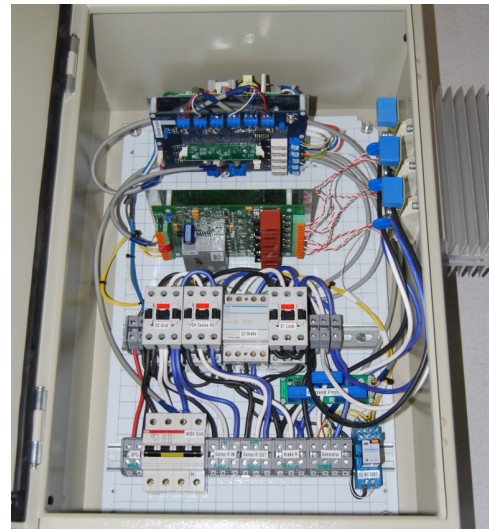


Fig. 14. Synchronisation controller box. Thyristors and heat-sink shown in upper right of frame

V. IMPLEMENTATION AND TESTING

A. Hardware Development

The SC is based around a Texas Instruments *F28027* MCU and is illustrated in Fig. 14. A Semikron *RT380T* controller is used to produce the requisite firing pulses for a W3C thyristor set, also from Semikron.

It was found that thyristor firing within a certain α range is inconsistent – most likely the result of false zero-crossing detections by the *RT380T* due to the high harmonic content

of the voltage waveforms. This issue is as yet unresolved but solutions which are under investigation include the use of a different thyristor controller, filtering of the voltage signals received by the controller, and smoothing of the S-PMG terminal voltage with power capacitors.

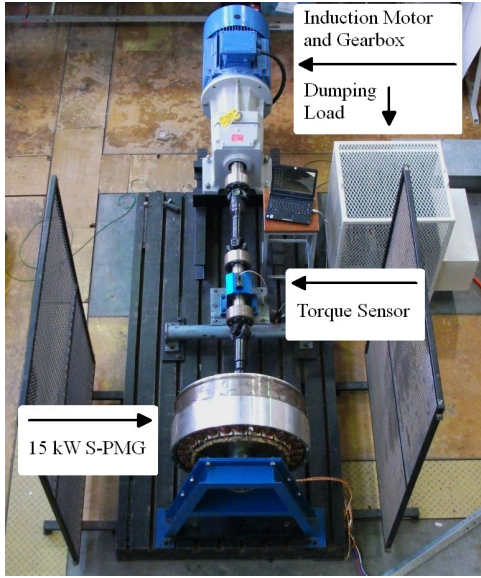


Fig. 15. S-PMG test rig with dumping load

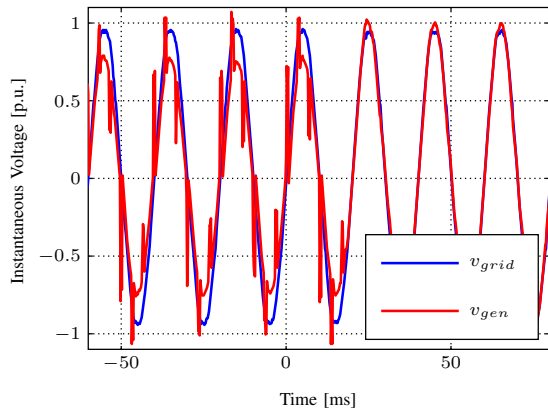


Fig. 16. Measured phase voltage waveforms during synchronization at rated torque. Sync. signal given at $t = 0$ s. Contactor closed at $t = 0.014$ s

B. Experimental Design Verification

Synchronization and speed control were investigated on a test bench, shown in Fig. 15. A 15 kW S-PMG is driven by a 45 kW geared induction motor fed by a 37 kW Allen-Bradley *Powerflex* variable speed drive (VSD), which is controlled to simulate the turbine. A Lorenz *DR-2212* in-line torque sensor logs input torque from the gear-motor. The dumping load (R_d) was constructed from industrial heating elements.

1) *Synchronization*: Synchronization experiments were performed at rated torque with the SC operating according to the tolerance limits set in Section III. The measured phase voltages are shown in Fig. 16 and the resulting phase current is illustrated in Fig. 17. The corresponding simulated waveforms are shown in Figs. 18 and 19. Very close agreement is achieved between experiment and simulation, as well as with the prediction of with Fig. 8c. The SC design and implementation are thus shown to be successful.

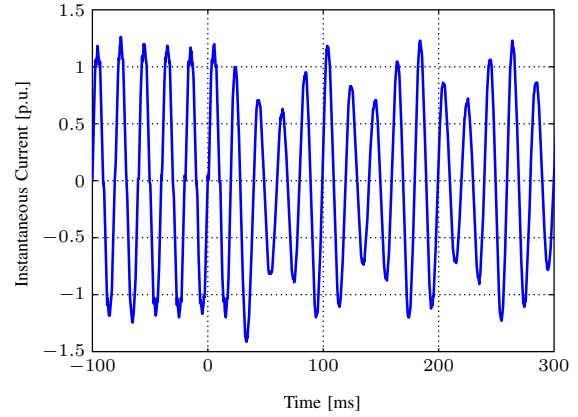


Fig. 17. Measured phase current waveform during synchronization at rated torque. Sync. signal given at $t = 0$ s. Contactor closed at $t = 0.014$ s

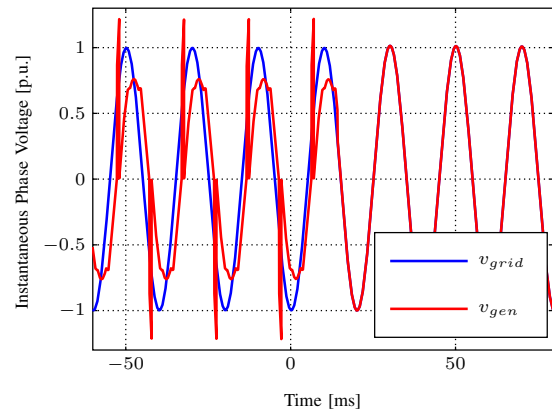


Fig. 18. Simulated phase voltage waveforms during synchronization at rated torque. Sync. signal given at $t = 0$ s. Contactor closed at $t = 0.014$ s

2) *Speed Control*: Due to an unstable interaction between the SC speed controller and that of the VSD, the full gain values of Section IV could not be successfully applied in the experimental system. To validate the simulation model, reduced gains were used in both the experiment and simulation, and the performance was compared for a steady 8 m/s wind.

Fig. 20 shows that the maximum overshoot and settling times agree well between the simulated and experimental cases. The ramp rate differs substantially due to difficulties in configuring the VSD to accurately emulate the behaviour of a turbine. A custom-built VSD is currently under development to better simulate the turbine and allow for complete tests of the speed control, including turbulent wind conditions. Results obtained thus far do, however, suggest that the simulation model can be relied upon for control design purposes.

VI. CONCLUSION

This paper detailed a proposed design for the synchronization controller (SC) that forms an essential part of the direct-to-grid S-PMG concept introduced in [2]. This approach to grid connection has not previously, to the authors' knowledge, been documented in literature for small-scale (sub-100 kW) WTGs.

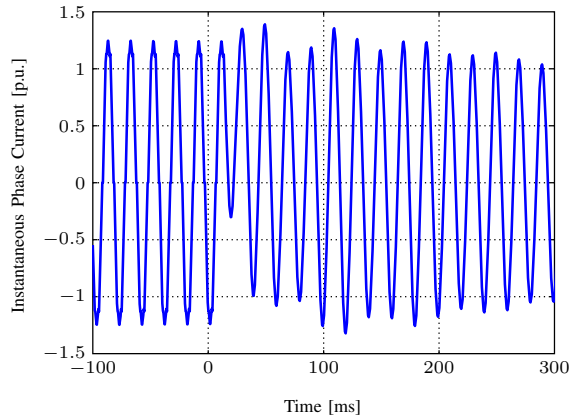


Fig. 19. Simulated phase current waveform during synchronisation at rated torque. Sync. signal given at $t = 0$ s. Contactor closed at $t = 0.014$ s

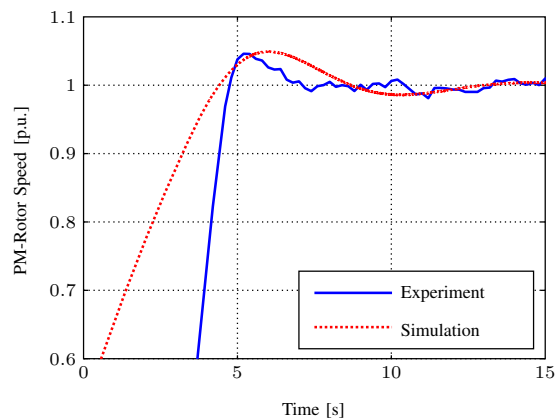


Fig. 20. Comparison of experimental and simulated results for PI speed control with 80% reduced gains and $V_{wind} = 8$ m/s

The S-PMG has favourable characteristics for use in the developing world, namely grid voltage support capabilities, affordability and minimal maintenance requirements. These characteristics also make the system appealing for remote mini-grids and even off-shore installations, if the concept is scaled up into the megawatt range.

The characteristics and operating principles of the S-PMG system were discussed before the modelling of the S-PMG was explained. The hardware implementation and the experimental test rig were also described.

With the synchronisation methodology and condition evaluation algorithm laid out, tolerance limits (f_t and ϕ_t) were established to ensure successful synchronisation throughout the usable wind speed range. The operation of the synchronisation algorithm was validated by experiments, where good agreement with predictions was achieved.

Speed control is facilitated by electrical braking through a resistive load. The contactor-based control approach was shown to be conditionally feasible, depending upon local wind conditions. The thyristor-based speed control was shown to achieve good dynamics throughout the operational wind speed range in simulations. Design validation through experiments

could not be completed due to implementation issues, but preliminary results showed performance similar to that obtained in simulations.

The findings presented here indicate that the direct-to-grid S-PMG concept is a promising candidate for further development. It is possible to achieve direct grid connection in a stable and automated manner, throughout the operational wind speed range.

REFERENCES

- [1] S. Reddy and J. P. Painuly, "Diffusion of renewable energy technologies – barriers and stakeholders' perspectives," *Renewable Energy*, vol. 29, no. 9, pp. 1431 – 1447, 2004. [Online]. Available: <http://www.sciencedirect.com/science/article/B6V4S-4BWW9VH-1/2/45362da7083bda0ce63c070af9d7160e>
- [2] J. Potgieter and M. Kamper, "Design of new concept permanent magnet induction wind generator," in *IEEE Energy Conversion Conf. and Expo. (ECCE)*, Atlanta, Georgia, USA, Sep 2010, pp. 2403 –2408.
- [3] P. Tavnet, G. V. Bussel, and F. Spinato, "Machine and converter reliabilities in wind turbines," in *3rd IET Conf. on Power Electron., Mach. and Drives*, Dublin, Ireland, Mar 2006, p. 127 130.
- [4] P. Bouwer, J. Potgieter, and M. Kamper, "Modelling and dynamic performance of a direct-drive direct-grid slip permanent magnet wind generator," in *IEEE Int. Elect. Mach. and Drives Conf. (IEMDC) 2011*, Niagara Falls, Canada, 15 - 18 May 2011.
- [5] E. Welfonder, R. Neifer, and M. Spanner, "Development and experimental identification of dynamic models for wind turbines," *Elsevier Control Eng. Practice*, vol. 5, no. 1, pp. 63 – 73, 1997.
- [6] O. Wasynczuk, D. Man, and J. Sullivan, "Dynamic behaviour of a class of wind turbine generators during random wind fluctuations," *IEEE Trans. Power App. Syst.*, vol. 100, no. 6, pp. 2837 – 2845, 1981.
- [7] A. Westlake, J. Bumby, and E. Spooner, "Damping the power-angle oscillations of a permanent-magnet synchronous generator with particular reference to wind turbine applications," *IEE Proc. Elect. Power Applicat.*, vol. 143, no. 3, pp. 269 – 280, 1996.
- [8] H. Mueller, M. Poeller, A. Basteck, M. Tilscher, and J. Pfister, "Grid compatibility of variable speed wind turbines with directly coupled synchronous generator and hydro-dynamically controlled gearbox," in *Sixth Int. Workshop on Large-Scale Integration of Wind Power and Transmission Networks for Offshore Wind Farms*, Delft, Netherlands, Oct 2006, pp. 307 – 315.
- [9] S. Grabic, N. Celanovic, and V. Katic, "Permanent magnet synchronous generator cascade for wind turbine application," *IEEE Trans. Power Electron.*, vol. 23, no. 3, pp. 1136 –1142, May 2008.
- [10] J. Stegmann and M. Kamper, "Economic and efficiency evaluation of different battery charging wind generator systems," in *19th Southern African Universities Power Eng. Conf.*, Johannesburg, South Africa, Jan 2010, pp. 205 – 210.
- [11] S. Kelouwani and K. Agbossou, "Nonlinear model identification of wind turbine with a neural network," *IEEE Trans. Energy Convers.*, vol. 19, no. 3, pp. 607 – 612, Sep 2004.
- [12] N. Stannard and J. Bumby, "Performance aspects of mains connected small scale wind turbines," *IET Generation, Transmission & Distribution*, vol. 1, no. 2, pp. 348 – 356, 2007.
- [13] International Electrotechnical Commission, *Tech. Report 60725: Consideration of reference impedances and public supply network impedances for use in determining disturbance characteristics of electrical equipment having a rated current less than or equal to 75 A per phase*. Geneva, Switzerland: IEC, 2005.
- [14] T. Davies, C. Jefferson, and R. Mayer, "Automated synchronisation," in *IEE Colloq. on Microcomputer Instrumentation and Control Syst. in Power Electron.*, London, 1988.
- [15] E. Hinrichsen and P. Nolan, "Dynamics and stability of wind turbine generators," *IEEE Trans. Power App. Syst.*, vol. 101, no. 8, pp. 2640 – 2648, August 1982.
- [16] L. Gonzalez, E. Figueres, G. Garcera, O. Carranza, and F. Gonzalez-Espin, "Synchronization techniques comparison for sensorless control applied to wind energy conversion systems (WECS)," in *13th European Conf. on Power Electron. and Applicat. (EPE '09)*, Sep. 2009, pp. 1 –9.